

Physical properties in hole-doped $\text{SrFe}_{2-x}\text{Cu}_x\text{As}_2$ single crystals

Y. J. Yan, P. Cheng, J. J. Ying, X. G. Luo, F. Chen, H. Y. Zou,

A. F. Wang, G. J. Ye, Z. J. Xiang, J. Q. Ma, and X. H. Chen^{1*}

*Hefei National Laboratory for Physical Science at Microscale and Department of Physics,
University of Science and Technology of China, Hefei, Anhui 230026, People's Republic of China*

(Dated: June 9, 2021)

We report the structural, magnetic and electronic transport properties of $\text{SrFe}_{2-x}\text{Cu}_x\text{As}_2$ single crystals grown by self-flux technique. SrCu_2As_2 and SrFe_2As_2 both crystallize in ThCr_2Si_2 -type (122-type) structure at room temperature, but exhibit distinct magnetic and electronic transport properties. The x-ray photoelectron spectroscopy(XPS) Cu-2*p* core line position, resistivity, susceptibility and positive Hall coefficient indicate that SrCu_2As_2 is an *sp*-band metal with Cu in the $3d^{10}$ electronic configuration corresponding to the valence state Cu^{1+} . The almost unchanged Cu-2*p* core line position in $\text{SrFe}_{2-x}\text{Cu}_x\text{As}_2$ compared with SrCu_2As_2 indicates that partial Cu substitutions for Fe in SrFe_2As_2 may result in hole doping rather than the expected electron doping. No superconductivity is induced by Cu substitution on Fe sites, even though the structural/spin density wave(SDW) transition is gradually suppressed with increasing Cu doping.

PACS numbers: 74.70.Xa; 74.25.F-; 74.62.Dh

I. INTRODUCTION

Exploration of new high-temperature superconductors and research on their superconducting mechanism have always been the highlight in condensed matter physics. Especially the discovery of a second class of high-temperature superconductors - iron-based superconductors, has reignited the boom of the high-temperature superconductivity research. There are five types of iron-based superconductors: 1111 with ZrCuSiAs -type structure, 122 with ThCr_2Si_2 -type structure, 111 with Fe_2As -type structure, 11 with anti- PbO -type structure, and a newly discovered $\text{K}_x\text{Fe}_{2-y}\text{Se}_2$ with Fe vacancy which is called 122* structure. Among these materials, compound with 122 structure has gained much attention because of the high superconducting temperature and easiness to obtain large high quality single crystals.

In the 122-type compound BaFe_2As_2 , superconductivity can be induced by applying pressure[1–3], and by substitutions at the Ba site (by K)[4], at the Fe site (by Co, Ni, Ru, Rh, and Pd)[5, 6], and at the As site (by P)[7]. It has been revealed that partial Co, Ni, Rh and Pd substitutions at the Fe site in BaFe_2As_2 could induce superconductivity[8–11] with T_c up to 25 K whereas no superconductivity is induced by Mn[12–14] or Cr [15, 16] substitutions. As we know, the formal valence states of the atoms in BaFe_2As_2 are assigned as Ba^{2+} , Fe^{2+} and As^{3-} , so the Fe atoms are formally in the $3d^6$ electronic configuration. So it means that while electron doping at the Fe sites by Co, Ni with more $3d$ electrons induces superconductivity, hole doping by Cr, Mn with less $3d$ electrons does not. From this point of view, divalent copper Cu^{2+} with three more d -electrons than Fe should be a strong electron dopant for iron arsenide

superconductors. However, even though the Cu doping successfully suppresses the structural/SDW transition of the parent compound[17], superconductivity was not observed in the Cu-doped BaFe_2As_2 . It is a very strange phenomenon that doping Cu into iron-based superconductors shows a completely different character from that of doping with Co and Ni. Electronic structure calculations for SrCu_2As_2 and BaCu_2As_2 by Singh[18] predicted that these compounds might be *sp*-band metals with the Cu atoms having a formal valence state of Cu^{1+} and a nonmagnetic and chemically inert $3d^{10}$ electronic configuration. Therefore, we speculate that the distinct valence state of Cu ions may be the main reason for the different behavior compared with other transition metal doped condition.

To obtain insights into the nature of the puzzling properties of Cu-doped iron-based materials, we have synthesized a series of $\text{SrFe}_{2-x}\text{Cu}_x\text{As}_2$ single crystals and investigated their valence state of copper ions by XPS measurement, and their structural, magnetic and electronic transport properties.

II. MATERIALS AND METHODS

A series of $\text{SrFe}_{2-x}\text{Cu}_x\text{As}_2$ single crystals, from SrFe_2As_2 ($x=0$) to SrCu_2As_2 ($x=2.0$) were grown by self-flux technique using high purity Sr, Cu, Fe and As. Pre-reacted CuAs and FeAs were used as flux. For the growth of $\text{SrFe}_{2-x}\text{Cu}_x\text{As}_2$, the Sr and FeAs, CuAs flux with a molar ratio of $1:2.5(2-x):2.5x$ were placed into alumina crucibles and sealed inside evacuated quartz tubes. The crystal growth was carried out by heating the samples to 1150°C , holding there for 24 h and then cooling to 850°C at a rate of 2°C/h . The sizes of the obtained single crystals for $0 \leq x < 1.0$ were typically $5 \times 3 \times 0.15 \text{ mm}^3$, while that for $1.0 \leq x \leq 2.0$ were typically $2.5 \times 2 \times 0.15 \text{ mm}^3$.

^{*}Corresponding author; Electronic address: chenxh@ustc.edu.cn

The samples were characterized by x-ray diffraction (XRD) using Rigaku D/max-A x-ray diffractometer with Cu K_α radiation in the range of 10° - 70° with the step of 0.01° at room temperature. The actual Cu and Fe concentration of the single crystals were determined from energy-dispersive x-ray (EDX) analysis. The Cu content x used in this article is the actual composition determined by EDX. The valence state of Cu is determined by x-ray photoelectron spectroscopy (XPS). The resistivity was measured using the standard four-probe method by Quantum Design Physical Property Measurement System (PPMS). Hall resistivity data were collected using the ac transport option of a quantum design physical property measurement system in a four-wire geometry with switching the polarity of the magnetic field $H \parallel c$ to remove any magnetoresistive components due to the misalignment of the voltage contacts. Magnetic susceptibility was measured using Vibrating Sample Magnetometer (VSM).

III. RESULTS AND DISCUSSION

Figure 1(a) shows the single crystal XRD patterns for all the $\text{SrFe}_{2-x}\text{Cu}_x\text{As}_2$ single crystals, and only (00l) diffraction peaks are observed, indicating that the single crystals are in perfect (001) orientation. Fig. 1(b) shows the evolution of the lattice parameters of a- and c-axis as a function of Cu doping content. The lattice parameter of c-axes is obtained from the (00l) diffraction peaks, while that of a-axes is obtained by powder XRD. With increasing Cu doping content, the lattice parameter of a-axes increases monotonically, while that of c-axes decreases monotonically. The unit cell volume $V = a^2c$ firstly increases with increasing Cu content, reaches a maximum at about $x \sim 1.0$, and then decreases with further increasing Cu content. Obviously, the evolution of V for $\text{SrFe}_{2-x}\text{Cu}_x\text{As}_2$ shows a qualitative deviation from Vegard's law, which shows a linear decrease with Cu content. Ni *et al.*[17] reported the lattice parameters a and c and the unit cell volume V of $\text{Ba}(\text{Fe}_{1-x}\text{Cu}_x)_2\text{As}_2$ versus x up to $x=0.35$, which shows a similar evolution of V to $\text{SrFe}_{2-x}\text{Cu}_x\text{As}_2$. Singh[18] gave theoretical prediction that Cu in BaCu_2As_2 and SrCu_2As_2 has a fully occupied stable d^{10} shell at high binding energy, which means that the valence state of Cu in these compounds is +1. While in SrFe_2As_2 , the valence state of Fe is +2. Therefore, we conclude that the anomalous behavior of V of $\text{SrFe}_{2-x}\text{Cu}_x\text{As}_2$ may indicate interesting changes of valence state in the Cu/Fe sites. In order to confirm it, we performed XPS measurement on several samples, and the results are shown in Fig. 2. As shown in Fig. 2, the $\text{Cu}2p_{1/2}$ and $\text{Cu}2p_{3/2}$ binding energy maxima for Cu metal are about 951.9 eV and 932.0 eV, and the linewidths are very narrow. The lines in $\text{SrFe}_{2-x}\text{Cu}_x\text{As}_2$ single crystals are a little broader than that in Cu metal, and have positions nearly the same as that in Cu metal, which is the condition of Cu_2O as re-

ported previously[19]. While for CuO , the lines for divalent copper are distinctly different. Compared with that of Cu metal, the lines in CuO shift to higher binding energies, the linewidth is broader with a factor of 2, and also the satellite is very intense. Considering these distinct differences, the valence of Cu ions in $\text{SrFe}_{2-x}\text{Cu}_x\text{As}_2$ single crystals is monovalent, regardless of doping level.

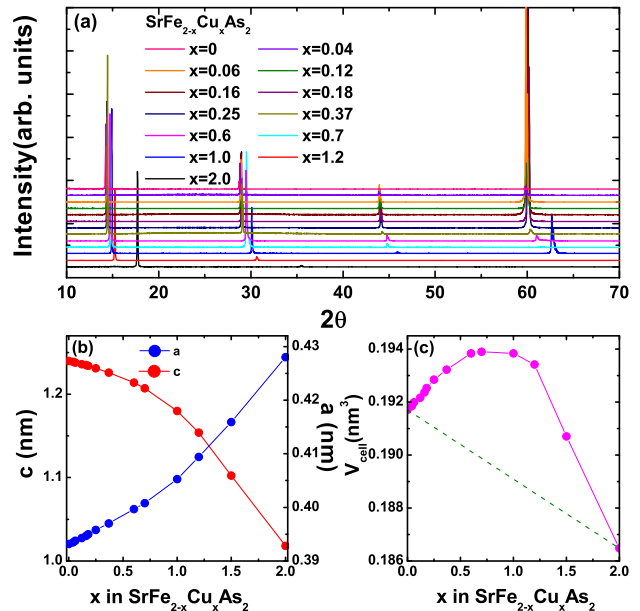


FIG. 1: (Color online)(a): Single crystal x-ray diffraction patterns at room temperature for $\text{SrFe}_{2-x}\text{Cu}_x\text{As}_2$ single crystals (x is the actual composition covering from 0 to 2.0.). Only (00l) diffraction peaks are observed, indicating that the c axis is perpendicular to the plane of the single crystal. (b): Lattice parameters of a- and c-axis as a function of x . The lattice parameters of a- and c-axis were obtained by combining single crystal XRD and powder XRD patterns. The data for $x=1.5$ are collected from polycrystal. (c): The unit cell volume V as a function of x for $\text{SrFe}_{2-x}\text{Cu}_x\text{As}_2$ single crystals. The green dashed line represent Vegard's law for this series of compounds.

The temperature dependence of in-plane electrical resistivity for $\text{SrFe}_{2-x}\text{Cu}_x\text{As}_2$ single crystals are shown in Fig. 3. As shown in Fig. 3(a), the resistivity exhibits obvious anomaly at the temperature from 196 K for SrFe_2As_2 to 71 K for the samples slightly doped with Cu, which is associated with structural/SDW transition reported previously[20]. The temperature of structural/SDW transition, T_{SDW} , decreases with increasing Cu doping, and disappears when $x > 0.25$. The anomaly due to the structural/SDW transition becomes more pronounced with doping, which is similar to that of Mn or Cr doped BaFe_2As_2 [8, 14], and in strong contrast with Co or Ni doped BaFe_2As_2 [6]. Fig. 3(b) shows the temperature dependence of resistivity for $0.37 \leq x \leq 1.2$ samples. The value of resistivity decreases quickly with increasing Cu doping, and the behavior of resistivity evolves from semi-

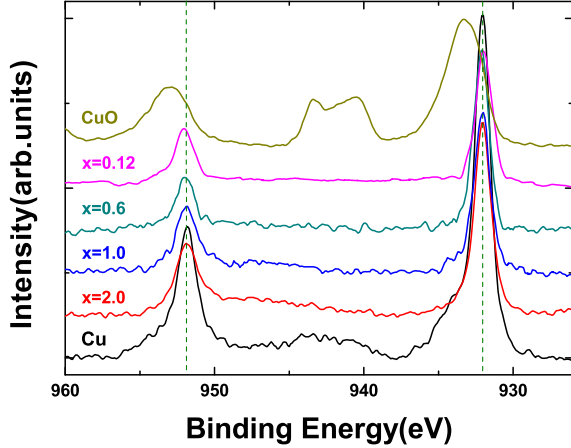


FIG. 2: (Color online) XPS Cu - $2p$ spectra of Cu metal (where Cu is nominally in a Cu^{0+} state), CuO (where Cu is in a Cu^{2+} state) and $\text{SrFe}_{2-x}\text{Cu}_x\text{As}_2$ single crystals with $x=0.12, 0.6, 1.0, 2.0$ after background subtraction. The two dashed lines correspond to the binding energies of Cu - $2p_{1/2}$ and Cu - $2p_{3/2}$ in Cu metal.

conducting to metallic-like and no anomaly is observed due to the structural or magnetic transition. For the samples $x=0.37, 0.6, 0.7$, the temperature dependence of resistivity shows semiconducting behavior in the whole temperature range. While for $x=1.0$, the resistivity exhibits metallic behavior above 190 K, and then turns into semiconducting behavior. For $x=1.2$, the resistivity is $0.19 \text{ m}\Omega \text{ cm}$ at 300 K, which is one order of magnitude larger than that of SrCu_2As_2 . The resistivity decreases with cooling, reaches a minimum at around 20 K, and then turns upward. The resistivity of SrCu_2As_2 as a function of temperature is presented in Fig. 3(c), which is similar to the results reported previously[21]. The temperature coefficient of $\rho(T)$ is positive, indicating metallic character. The values of residual resistivity ρ_0 and residual resistivity ratio(RRR) are $4.2 \mu\Omega \text{ cm}$ and 6.4, respectively, indicating good quality of SrCu_2As_2 single crystals. The clear evolution of the resistivity behavior and phase transition are shown in Figs. 3(d) and 3(e).

Figure 4 presents the zero-field-cooled (ZFC) or field-cooled(FC) magnetic susceptibility χ for all the single crystals as a function of temperature from 2 K to 300 K in an applied magnetic field $H=5.0 \text{ T}$ aligned in the ab plane. Fig. 4(a) presents the typical behavior of one SrFe_2As_2 single crystal before and after an annealing at 300°C for 5 hours. The temperature dependence of χ exhibits an unusual behavior for the as-grown SrFe_2As_2 , and changes to a universal behavior after annealing, which is consistent with the previous report[22]. These phenomena are supposed to be related to the presence of lattice distortion in SrFe_2As_2 [23]. For samples with $0 \leq x \leq 0.25$ as shown in Figs. 4(a) and 4(b), structural/SDW transition is obviously observed and marked

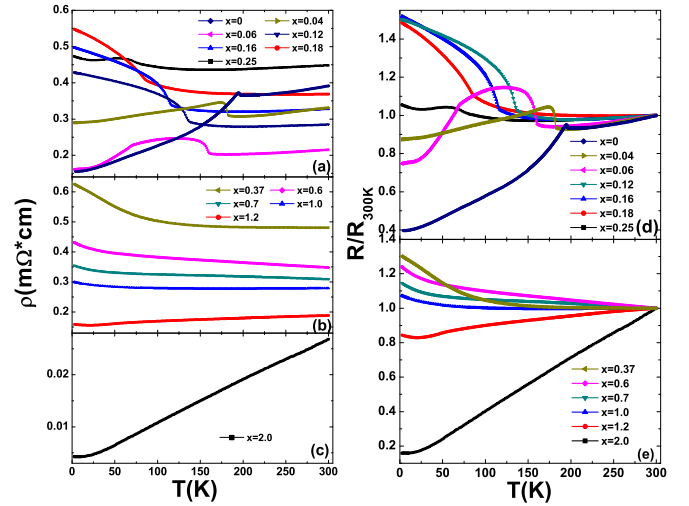


FIG. 3: (Color online) (a)-(c): Temperature dependence of plane electrical resistivity for $\text{SrFe}_{2-x}\text{Cu}_x\text{As}_2$ single crystals. (d) and (e): Temperature dependence of the normalized resistivity to 300 K.

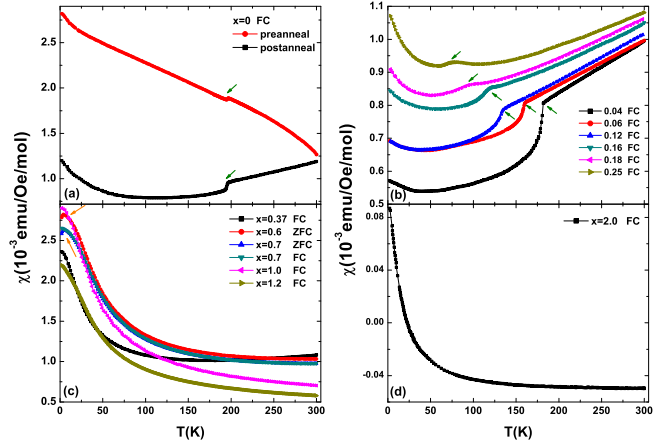


FIG. 4: (Color online) Temperature dependence of magnetic susceptibility for $\text{SrFe}_{2-x}\text{Cu}_x\text{As}_2$ ($0 \leq x \leq 2.0$) under magnetic field of 5T. The SDW transition temperature T_{SDW} is shown by green arrows. The orange arrow shows the spin glass-like transition.

by green arrows, corresponding to the anomaly observed in the resistivity shown in Figs. 3(a) and 3(d). The $\chi(T)$ of samples with $0.37 \leq x \leq 1.2$ show paramagnetic behavior in the whole temperature range, and no obvious magnetic transition was observed down to 2 K. The magnitude of χ decreases with increasing Cu doping as shown in Fig. 4(c). Below 20 K, a small separation between FC and ZFC curves for the crystal with $x=0.7$ is observed, indicating glass-like behavior. The χ of SrCu_2As_2 in Fig. 4(d) has a negative sign above 20 K, which is a typical behavior for nonmagnetic metal and is consistent with

the previous report[21].

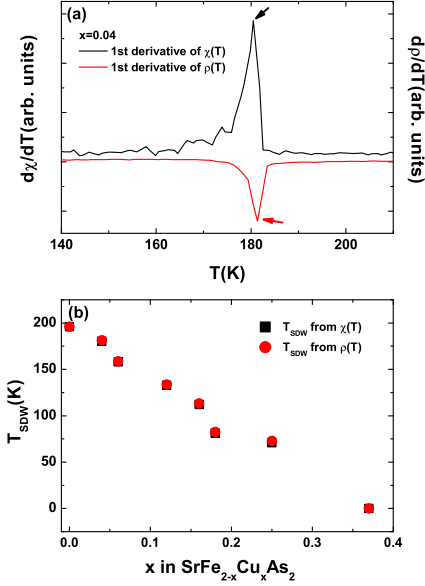


FIG. 5: (Color online)(a): The derivatives of $\chi(T)$ and $\rho(T)$ as a function of temperature for $x=0.04$ sample. The distinct peaks indexed by arrows in $d\chi(T)/dT$ and $d\rho(T)/dT$ curves are used to determine the temperature of structural/SDW transition. (b): Evolution of T_{SDW} with Cu doping.

Figure 5(a) shows the typical derivatives of $\chi(T)$ and $\rho(T)$ to figure out the transition temperature T_{SDW} of structural/SDW transition. Only one obvious peak is observed in both derivative curves of $\chi(T)$ and $\rho(T)$, corresponding to the temperature of phase transition. T_{SDW} determined from derivatives of $\chi(T)$ and $\rho(T)$ are highly consistent with each other, as shown in Fig. 5(b). With increasing Cu doping, T_{SDW} decreases quickly from 196 K for $x=0$ to 71 K for $x=0.25$, which is similar to that of $\text{Ba}(\text{Fe}_{1-x}\text{Cu}_x)_2\text{As}_2$ [17], except that no superconductivity was observed in $\text{SrFe}_{2-x}\text{Cu}_x\text{As}_2$ for any doping content.

To further understand the conducting carriers in the Cu-doped SrFe_2As_2 samples, the Hall coefficient (R_H) measurements were carried out on the single crystals, and the obtained results are shown in Fig. 6. In Figs. 6(a) and 6(b), distinct structural/SDW transition can be observed for samples $0 \leq x \leq 0.18$, consistent with the resistivity and susceptibility. The Hall coefficient is negative indicating electron-type carriers dominate, and the absolute value decreases with Cu doping content. For $0.25 \leq x \leq 1.2$, the Hall coefficients R_H are also negative in the whole temperature range, indicating that the dominated carrier is electron-type. The absolute value of Hall coefficients for $x=0.25$ and 0.37 are smaller than that of samples with lower Cu doping content. It increases with cooling, reach minima at around 40 K, and then weakly decline at low temperature. For $x=0.25$, no phase transition is observed around the temperature corresponding to

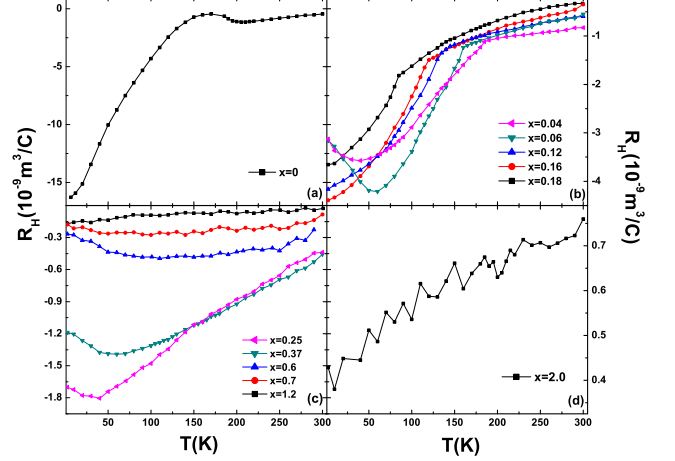


FIG. 6: (Color online) Temperature dependence of Hall coefficients R_H for $\text{SrFe}_{2-x}\text{Cu}_x\text{As}_2$ samples.

structural/SDW transition, probably because its phase transition is too weak. A weak temperature dependence of Hall coefficient is observed in the whole temperature region for samples $x=0.6, 0.7$ and 1.2 . The absolute values of R_H for these three samples are very small with the same order of magnitude of $10^{-10} \text{ m}^3/\text{C}$, and decreases with further increasing Cu doping. As shown in Fig. 6(d), it is clear that the Hall coefficient of SrCu_2As_2 is positive in the whole temperature range, which suggests that the hole-type carriers dominate. The value of R_H is $7 \times 10^{-10} \text{ m}^3/\text{C}$ at 300 K, which is remarkably small, indicating a relatively high density of charge carriers estimated to be of the order of 10^{22} cm^{-3} . The magnitude and temperature dependence of Hall coefficient for SrCu_2As_2 is similar to the reports by Qin et al.[24]. In conclusion, with the gradual increase of Cu doping, the Hall coefficient changes from negative to positive, and its absolute value changes gradually. These results indicate that the carrier changes from electron-type to hole-type, and the concentration of carrier changes simultaneously with Cu content. Combining with XPS results, it strongly suggests that partial Cu substitutions for Fe in SrFe_2As_2 may result in hole doping rather than the expected electron doping. This is probably the reason that Cu substitutions in iron-based materials can not induce superconductivity.

To our knowledge, the valence state of Cu found in the previously reported pnictide oxides is always +1, because the anionic environment of the pnictide oxides is in general not sufficiently electronegative to oxidize Cu to +2. Even in the LaNiO_2 -type $[\text{M}^i\text{O}_2]$ layer of oxyulfides $\text{Sr}_2[\text{M}'_{1-x}\text{Cu}^{2+x}\text{O}_2][\text{Cu}^{1+2}\text{S}_2]$ ($\text{M}' = \text{Sc, Cr, Mn, Fe, Co, Ni, Zn}$), which are expected to have more electronegative anionic environment than the pnictide oxides, the maximum Cu^{2+} content for the single-phase sample was $x < 1$ [25, 26]. This also indicates that the accommoda-

tion of Cu^{2+} in the weakly electronegative anionic environment of suboxides such as pnictide oxides and oxychalcogenides is difficult in contrast to its accommodation in the more electronegative anionic environment of oxides[27]. Therefore, the valence state of Cu prefers +1 in the iron-based pnictide with more weakly electronegative anionic environment, such as in EuCuPn ($\text{Pn} = \text{P}, \text{As}, \text{Sb}$)[28], BaCuAs , CaCuAs , SrCu_2As_2 , SrCu_2Sb_2 , and BaCu_2Sb_2 [21].

IV. CONCLUSION

In summary, XPS Cu-2*p* spectra, deviation of *V* from Vegard's law, diamagnetic susceptibility, and positive Hall coefficient indicate that the valence state of Cu in SrCu_2As_2 is +1 with a fully occupied 3*d* shell. The struc-

tural/SDW transition is suppressed with increasing Cu doping content for $x \leq 0.25$, and disappears when Cu doping content *x* is higher than 0.25. Superconductivity can not be induced over the whole doping range. The nearly same Cu-2*p* core line position as that in SrCu_2As_2 for all crystals and the evolution of Hall coefficients strongly suggest that partial Cu substitutions for Fe in SrFe_2As_2 may result in hole doping rather than the expected electron doping, which is the possible reason for that Cu doping cannot induce superconductivity in the $\text{SrFe}_{2-x}\text{Cu}_x\text{As}_2$.

Acknowledgment: This work is supported by the National Natural Science Foundation of China, and the National Basic Research Program of China (973 Program, Grants No. 2012CB922002 and No. 2011CB00101), and the Chinese Academy of Sciences.

-
- [1] T. Yamazaki, N. Takeshita, R. Kobayashi, H. Fukazawa, Y. Kohori, K. Kihou, C. H. Lee, H. Kito, A. Iyo, and H. Eisaki, *Phys. Rev. B* **81**, 224511 (2010).
- [2] F. Ishikawa, N. Eguchi, M. Kodama, K. Fujimaki, M. Einaga, A. Ohmura, A. Nakayama, A. Mitsuda, and Y. Yamada, *Phys. Rev. B* **79**, 172506 (2009).
- [3] E. Colombier, S. L. Budko, N. Ni, and P. C. Canfield, *Phys. Rev. B* **79**, 224518 (2009).
- [4] H. Chen, Y. Ren, Y. Qiu, Wei Bao, R. H. Liu, G. Wu, T. Wu, Y. L. Xie, X. F. Wang, Q. Huang, X. H. Chen, *Europhys. Lett.* **85**, 17006 (2009).
- [5] D. C. Johnston, *Adv. Phys.* **59**, 803 (2010).
- [6] P. C. Canfield, and S. L. Budko, *Annu. Rev. Condens. Matter Phys.* **1**, 27 (2010).
- [7] S. Jiang, H. Xing, G. Xuan, C. Z. Ren, C. Feng, J. Dai, Z. Xu, and G. Cao, *J. Phys. Condens. Matt.* **21**, 382203 (2009).
- [8] A. S. Sefat, R. Jin, M. A. McGuire, B. C. Sales, D. J. Singh, and D. Mandrus, *Phys. Rev. Lett.* **101**, 117004 (2008).
- [9] C. Wang, Y. K. Li, Z. W. Zhu, S. Jiang, X. Lin, Y. K. Luo, S. Chi, L. J. Li, Z. Ren, M. He, H. Chen, Y. T. Wang, Q. Tao, G. H. Cao, and Z. A. Xu, *Phys. Rev. B* **79**, 054521 (2009).
- [10] X. F. Wang, T. Wu, G. Wu, R. H. Liu, H. Chen, Y. L. Xie and X. H. Chen, *New J. Phys.* **11**, 045003 (2009).
- [11] L. J. Li, Q. B. Wang, Y. K. Luo, H. Chen, Q. Tao, Y. K. Li, X. Lin, M. He, Z. W. Zhu, G. H. Cao, and Z. A. Xu, *New J. Phys.* **11**, 025008 (2009).
- [12] D. Kasinathan, A. Ormeci, K. Koch, U. Burkhardt, W. Schnelle, A. Leithe-Jasper, and H. Rosner, *New J. Phys.* **11**, 025023 (2009).
- [13] Y. Liu, D. L. Sun, J. T. Park, and C. T. Lin, *Physica C* **470**, S513 (2010).
- [14] J. S. Kim, S. Khim, H. J. Kim, M. J. Eom, J. M. Law, R. K. Kremer, J. H. Shim, and K. H. Kim, *Phys. Rev. B* **82**, 024510 (2010).
- [15] A. S. Sefat, D. J. Singh, L. H. VanBebber, Y. Mozharivskyj, M. A. McGuire, R. Jin, B. C. Sales, V. Keppens, and D. Mandrus, *Phys. Rev. B* **79**, 224524 (2009).
- [16] K. Marty, A. D. Christianson, C. H. Wang, M. Matsuda, H. Cao, L. H. VanBebber, J. L. Zarestky, D. J. Singh, A. S. Sefat, and M. D. Lumsden, *Phys. Rev. B* **83**, 060509(R) (2011).
- [17] N. Ni, A. Thaler, J. Q. Yan, A. Kracher, E. Colombier, S. L. Bud'ko, P. C. Canfield, and S. T. Hannahs, *Phys. Rev. B* **82**, 024519 (2010).
- [18] D. J. Singh, *Phys. Rev. B* **79**, 153102 (2009).
- [19] P. Steiner, V. Kinsinger, I. Sander, B. Siegwart, S. Hufner, C. Politis, R. Hoppe, and H. P. Müller, *Z. Phys. B - Condensed Matt.* **67**, 497 (1987).
- [20] A. Jesche, N. Caroca-Canales, H. Rosner, H. Borrmann, A. Ormeci, D. Kasinathan, H. H. Klauss, H. Luetkens, R. Khasanov, A. Amato, A. Hoser, K. Kaneko, C. Krellner, and C. Geibel, *Phys. Rev. B* **78**, 180504(R) (2008).
- [21] V. K. Anand, P. Kanchana Perera, Abhishek Pandey, R. J. Goetsch, A. Kreyssig, and D. C. Johnston, *Phys. Rev. B* **85**, 214523 (2012).
- [22] J.-Q. Yan, A. Kreyssig, S. Nandi, N. Ni, S. L. Budko, A. Kracher, R. J. McQueeney, R. W. McCallum, T. A. Lograsso, A. I. Goldman, and P. C. Canfield, *Phys. Rev. B* **78**, 024516 (2008).
- [23] S. R. Saha, N. P. Butch, K. Kirshenbaum, and Johnpierre Paglione, and P.Y. Zavalij, *Phys. Rev. Lett.* **103**, 037005 (2009).
- [24] Mingsheng Qin, Chongyin Yang, Yaoming Wang, Zhongtian Yang, Ping Chen, and Fuqiang Huang, *J. Solid State Chem.* **187**, 323 (2012).
- [25] S. Okada, M. Matoba, s. Fukumoto, S. Soyano, Y. Kamihara, T. Takeuchi, H. Yoshida, K. Ohoyama, and Y. Yamaguchi, *J. Appl. Phys.* **91**, 8861 (2002).
- [26] H. Hirose, K. Ueda, H. Kawazoe, and H. Hosono, *Chem. Mater.* **14**, 1037 (2002).
- [27] T. C. Ozawa, and S. M. Kauzlarich, *Sci. Technol. Adv. Mater.* **9**, 033003 (2008).
- [28] G. Michels, S. Junk. W. Schlabit, E. Holland-Moritz, M. M. AbdElmeguid, J. Dünner, and A Mewis, *J. Phys.: Condens. Matter* **6**, 1769 (1994).